The average shape of large waves in the coastal zone

C. N. Whittaker[a,*], A. C. Raby[b], C. J. Fitzgerald[c], P. H. Taylor[c]

[a] *Department of Civil and Environmental Engineering, Faculty of Engineering, University of Auckland, Symonds St, Auckland 1010, New Zealand*
[b] *Department of Marine Science and Engineering, Faculty of Science and Environment, Plymouth University, Drake Circus, PL4 8AA, UK*
[c] *Department of Engineering Science, University of Oxford, Parks Rd, Oxford OX1 3PJ, UK*

Abstract

The ability of the NewWave focused wave group (the scaled auto-correlation function) to represent the average shape in time of large waves in a random sea state makes it a useful tool for the design of offshore structures. However, the profile has only been validated against field data for waves on deep and intermediate water depth. A similar validation is advisable when applying NewWave to shallow water problems, where waves are less dispersive and more nonlinear. For this purpose, data recorded by two Channel Coastal Observatory (CCO) wave buoys during two large storms in January 2014 are analysed to assess the ability of NewWave to replicate the average shape of large waves in shallow water. A linear NewWave profile is shown to successfully capture the average shape of the largest waves from the Perranporth and Porthleven wave buoys during these large storm events. The differences between the measurements obtained by a surface-following buoy and a fixed sensor become important when considering the ability of a second-order corrected NewWave profile to capture weakly nonlinear features of the measured data. A general expression for this effect is presented for weakly nonlinear waves on intermediate water depths, leading to Lagrangian second-order sum corrections to the linear NewWave profile. A second-order corrected NewWave profile performs reasonably well in capturing the average features of large waves recorded during the January storms. These findings demonstrate that the NewWave profile is valid in relatively shallow water (k_pD values less than 0.5), and so may have potential for use as a design wave in coastal engineering applications.

Keywords: Wave buoy data, Shallow water waves, NewWave

*Corresponding author
Email address: c.whittaker@auckland.ac.nz (C. N. Whittaker)

1. Introduction

Large waves pose a significant threat to people and assets located close to the coastline, particularly due to their ability to overtop or even demolish flood defences during severe storms. The winter storms of 2013/2014 demonstrated the vulnerability of UK coastal communities to wave attack. The effect of these storms was amplified when the waves broke a major rail link so that rail services stopped for three months. The danger of wave attack (and subsequent overtopping of structures) is likely to increase in the future, due to rising sea levels and possible increases in extreme climactic conditions. Facing these challenges, the design of robust coastal structures is a priority for coastal engineers worldwide.

Coastal defence structures are generally designed with the overarching assumption that wave attack should be modelled in a statistical manner. This approach is largely adopted due to the complexity of the coastal zone processes that affect the wave runup and overtopping, and the strong influence of the local bathymetry on these processes. Most design guidance therefore relies on empirical results obtained from a large number of tests (e.g. Geeraerts et al., 2007). However, these methods may only be able to provide an order of magnitude estimate of overtopping discharges and volumes on a wave by wave basis (see, for example, the EurOtop manual - Pullen et al., 2007). This uncertainty may lead to overly conservative design of coastal structures, while the exclusive use of random sea states in probabilistic tests may miss the physics of the individual wave properties that lead to extreme overtopping. Although it is difficult to directly relate a particular incident wave within a random wave train to instances of extreme wave-by-wave runup or overtopping at the shore (Hofland et al., 2014), there is certainly scope for further research in this area.

Abnormal (or rogue) waves are also of great interest to oceanographers, offshore/coastal engineers and applied mathematicians. These are generally defined as waves that are too large (and appear too often) to be consistent with Rayleigh-type statistics for a random wave field (see Adcock and Taylor, 2014, for a recent review). Although various driving mechanisms have been proposed, these rogue waves are often associated with the modulational instability of wave trains, consistent with particular values of the Benjamin Feir index (Janssen, 2003). However, as the basic driving instability disappears for waves on water shallower than $kD = 1.36$, this mechanism is unlikely to be relevant for the shallow water conditions considered in this paper. Experimental or numerical investigations into rogue waves will typically require long test durations to capture extremes within a random sea state.

An alternative to lengthy probabilistic experiments might be the use of a deterministic design wave chosen to represent an extreme event within a given sea state. By modelling the free surface elevation as a linear random Gaussian process, the average shape of a large crest may be described by the autocorrelation function of the process (Tromans et al., 1991; Boccotti, 1983). This is an asymptotic form of the full solution of Lindgren (1970) for a suitably large event within a given storm. For long-duration storms, the assumption of a linear Gaussian process may be violated by slow variations such as tides and surges. However, the resulting focused wave profile, often referred to as NewWave, has been demonstrated to capture accurately the average shape of large waves recorded at different offshore platforms in severe conditions (Jonathan and Taylor, 1997; Walker et al., 2004; Taylor and Williams, 2004; Santo et al., 2013).

The ability of the NewWave profile to provide a compact representation of an extreme wave event within a random sea state might allow large reductions in experimental and computational effort compared to random simulations/experiments, making it an attractive option in the study of coastal responses to wave attack. In addition to the time savings, the use of a compact wave group (such as NewWave) would avoid long wave re-reflections at experimental wavemakers (an issue in long-duration irregular wave tests). Although an isolated event is less applicable when investigating processes which occur over longer time scales (e.g. scour, sediment transport or infra-gravity wave generation), the NewWave profile may also be embedded in an irregular sea state to model the effect of an extreme event within the background process. This profile is therefore relevant to experimental or numerical investigations into structural responses to extreme incident wave conditions.

To date, NewWave has been validated against field data in deep and intermediate water depths, corresponding to nondimensional water depths (kD) between 1.6 and 3.5 (see Table 1). In these cases, linear frequency dispersion is the dominant process affecting wave structure and evolution, and the assumptions underlying the formulation of the NewWave profile are valid. However, the decreasing strength of frequency dispersion and increasing nonlinearity of waves in shallow water casts some doubt on the validity of the NewWave profile in runup and overtopping scenarios.

This paper aims to establish the validity of the NewWave profile for pre-breaking waves in locally severe conditions on relatively shallow water, using wave buoy data recorded in the southwest of the UK. The wave buoys under consideration are managed and operated by the Plymouth Coastal Observatory (PCO), and are described in Section 2. This section also discusses some of the issues encountered when attempting to extract wave-by-wave information from

Table 1: Previous application of NewWave to large waves recorded in the field.

Field data source	Location	D (m)	kD	H_s (m)	T_z (s)
Tern Platform	Northern North Sea	170	3.5	12.0	11.0
Hurricane Camille	Gulf of Mexico	100	2.2	13.3	13.7
Draupner Platform	Central North Sea	70	1.6	12.0	12.5
WACSIS Dataset	Southern North Sea	17	2.0	4.0	6.0

surface-following buoys. Section 3 presents the linear analysis method and results for two representative buoy records (captured during storm events) from Perranporth and Porthleven, and discusses the effect of the spectral shape on the results. Section 4 investigates the validity of a second-order corrected NewWave as an approximation to the (nonlinear) average profiles of large waves recorded by the buoys. This is initially achieved by considering second-order corrections to the NewWave profile and the effect of the Lagrangian motion of a wave buoy on wave records measured in shallow water. The ability of a phase- and amplitude-optimised NewWave profile to capture the shape of the nonlinear average large crest and trough profiles is then discussed. The results reported in this paper are intended to inform future experimental and numerical investigations into the use of localised wave groups like NewWave in the coastal zone, and their possible application to the design of coastal defence structures.

2. Wave measurements from the Channel Coastal Observatory buoy network

This section discusses the reasons for using wave buoy data to investigate the ability of NewWave to capture accurately the average shape of large waves in the coastal zone before introducing the Channel Coastal Observatory wave buoy data for this purpose. The locations and storms of interest are then discussed.

Obtaining accurate measurements of pre-breaking waves in relatively shallow water is a non-trivial exercise. Although simple to use in both small and large scale laboratory flumes, in the field surface-piercing measurement devices generally require a supporting structure, which can limit their deployment to oil and gas platforms in deep water or from the shoreline. Bottom-mounted pressure sensors may be used to measure waves in shallow water, but the recovery of free surface elevations from pressure measurements is problematic and tends to rely on either the assumption of linear wave theory or of hydrostatic pressure (see Constantin, 2014). Thus, neither surface-piercing instruments nor pressure transducers are considered in this study.

When appropriately moored, wave buoys may provide measurements within a full range of depths including relatively shallow water. However, at least historically, wave buoys have been used only for the collection of bulk statistics rather than for the analysis of individual waves. A moored wave buoy may travel around a large crest in a short-crested sea, or even be dragged through a large crest if it reaches the limit of its mooring line. These effects are not considered in this paper. Additionally, the Lagrangian buoy motion will still affect the wave measurements of an idealised buoy capable of perfectly following the free surface motions. Although the linear contributions to the free surface elevation measured by a surface-following and fixed sensor are equal, it is generally assumed that this Lagrangian motion will prevent the buoy from measuring the second harmonic component of steep deep-water waves obvious on a wave staff record (see James, 1986; Longuet-Higgins, 1986; Tucker and Pitt, 2001).

Previous comparisons between the NewWave profile and field data used Eulerian wave measurements in deep/intermediate water. However, the lack of Eulerian measurements in the coastal zone necessitates the use of wave buoy data for the current analysis. In the linear case, differences due to the measurement method should be small. The required modifications to the Eulerian theory used to analyse nonlinear wave buoy data are discussed in Section 4. In this section we show that (at second order) it is possible to recover some double frequency information. For a derivation of Eulerian second-order wave-wave interactions, the reader is referred to Dalzell (1999); Forristall (2000); Sharma and Dean (1981).

The Channel Coastal Observatory (CCO) comprises six regional coastal monitoring programmes within England. In the southwest (the area of interest for the current study) the programme is managed by the Plymouth Coastal Observatory (PCO), and includes the provision of free access to data from wave buoys and other sources with the broad aim of monitoring the coastal environment of the southwest (http://www.channelcoast.org/southwest/). Wave data are captured in 30 minute records containing the heave, northing and westing displacements of the buoy, though this study makes use of the heave record only. The sampling rate was fixed at 1.28 Hz within the analysed data. This relatively low frequency restricts the resolution of wave shapes, particularly shorter waves or bound double/sum frequency terms, as discussed in Section 3.

The buoy data were checked using the quality control procedures of Ashton and Johanning (2015), in order to remove the majority of the possible mechanical/electrical/processing errors in the buoy data. These sources of error, and the processing steps required to mitigate each source, are described in detail by Ashton (2012), and the reader is referred to this text for more

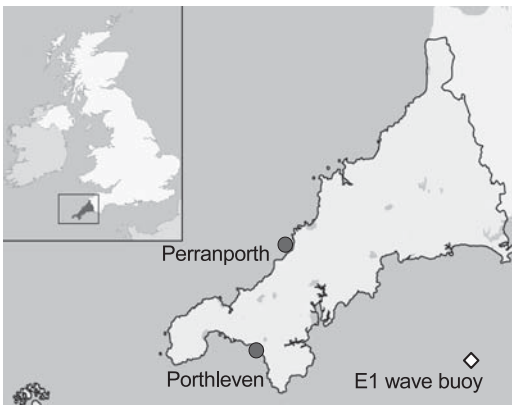

Figure 1: Locations of the Perranporth and Porthleven wave buoys, shown as dark circles, in the southwest of the UK.

information. As an additional quality control measure, the buoy data were high-pass filtered to remove energy at very low frequencies (as recommended by Ashton and Johanning, 2015).

Although wave buoy data records are available from a number of sites in this region, the current study considers only data from the Perranporth and Porthleven wave buoys (both Datawell Directional WaveRider Mk III buoys); the locations of these two wave buoys are shown in Figure 1, along with the offshore E1 buoy. The two locations have beaches that may be classified broadly as dissipative and reflective, based on their respective mild and steep slopes (see Scott et al., 2011, for a more detailed classification of beaches in this region). Comparisons between results from these two sites will provide an indication of the effect of the beach type on the analysis results (if any). The approximate operational depths for the buoys at the two sites were 10 m and 15 m respectively, i.e. very shallow water at both locations. Although these operational depths would vary during a tidal cycle, this variation is neglected in the analysis of the 30 minute buoy records.

The storms during the winter season of 2013/2014 generated very large waves that caused significant damage in the southwest of the UK. Wave records captured during these storms therefore provide a robust test of the effectiveness of the NewWave profile in capturing the average shape of large waves in the coastal zone. The Porthleven buoy was serviced on 30 January 2014, shortly before the storms of 5-6 February damaged several of the CCO wave buoys. To avoid these issues, while still considering large storm events, only records obtained before 30 January 2014 will be considered in the current analysis.

Table 2: Key parameters of Records 1a-2a (Perranporth buoy) and 1b-2b (Porthleven buoy) from the January 2014 storms.

Record no.	H_s (m)	f_p (Hz)	T_p (s)	k_pD	f_z (Hz)	T_z (s)	k_zD
1a	5.59	0.06	16.7	0.39	0.11	9.5	0.72
2a	5.34	0.05	20.0	0.32	0.09	10.6	0.64
1b	6.07	0.06	16.7	0.48	0.10	9.6	0.91
2b	6.37	0.05	20.0	0.40	0.10	10.2	0.84

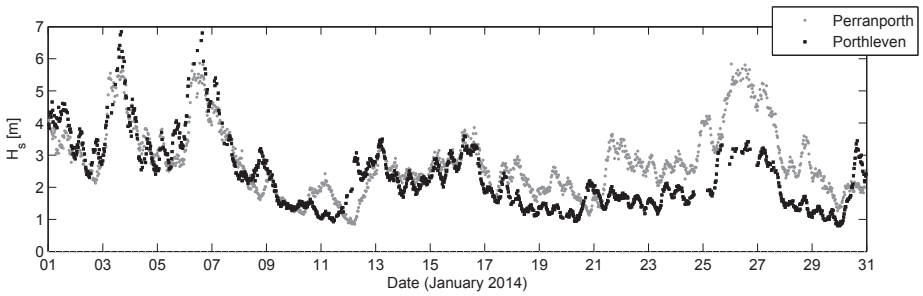

Figure 2: Variation in significant wave height measured by the Perranporth and Porthleven wave buoys during January, 2014.

Figure 2 shows the variation in the significant wave height measured by the Perranporth and Porthleven buoys during the month of January 2014. Records of interest were selected from the two largest storm events during this month, since these would provide suitably large waves in shallow conditions for the validation of the NewWave profile. These were recorded at 1900 on 03 January, and 1900 on 06 January; these are denoted Records 1a and 2a for the Perranporth buoy and Records 1b and 2b for the Porthleven buoy in this paper. Table 2 lists the significant wave heights (H_s), peak frequencies (f_p) and nondimensional water depths (k_pD, where k_p is the wavenumber corresponding to the peak frequency of the spectrum, f_p) for each of the four records, as well as the corresponding average zero-crossing properties f_z, T_z and k_zD. Section 3 first describes the analysis procedure using Record 1a (Perranporth buoy) as an example, then discusses the NewWave representation of the average large wave profiles for the four records.

3. NewWave representation of linearised large wave profiles

3.1. Creation of large linear wave profiles

Figure 3 shows the raw free surface elevation time series $\eta(t)$ of Record 1a from Perranporth, recorded from 1900 to 1930 on 03 January 2014. Previous studies using NewWave to examine

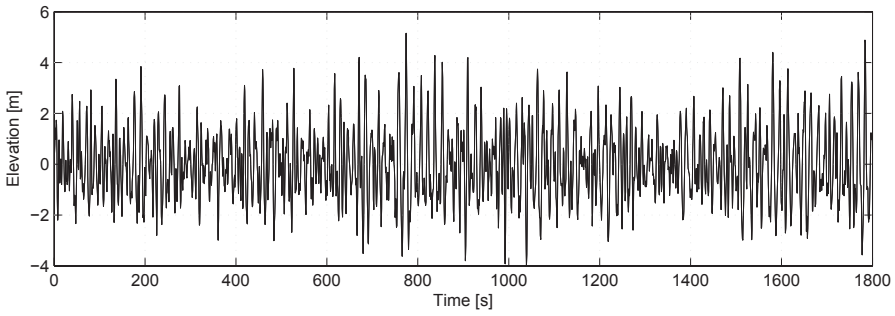

Figure 3: Free surface elevation time series measured at 1900 on 03 January, 2014, at Perranporth (Record 1a).

field data have typically created average profiles from a given number of the largest waves in the record, by creating short time series covering ±20 s around each extreme elevation point, setting the relative time of the extreme elevation to 0 s and then averaging across the short records. We follow the same procedure, creating average profiles from the largest 20 waves in each record (the records contained 181 waves on average). The validity of the autocorrelation function (hence NewWave) depends on the amplitudes of these large waves, and is discussed later in this section.

After their creation, the average profiles may be linearised using a separation of harmonics approach (see Walker et al., 2004). This approach is based on expansions in the weakly nonlinear harmonic series familiar in Stokes regular wave theory, and is based on symmetry arguments that are independent of spectral shape or bandwidth. For negligible third-order contributions, the linearised profile may be obtained by:

$$\eta_0^L = \frac{\eta_0 - \eta_{180}}{2}, \tag{1}$$

where the numeric subscripts represent the phase of the average large wave profile (in degrees) relative to the conditioning point in time, while the 'L' superscript denotes the linearised profile. Hence η_0^L is the linearised average large crest profile, η_0 is the average large crest profile and η_{180} is the average large trough profile. The variables of interest are defined in the Nomenclature Section at the end of the paper; in general, η is used for measured properties and y for theoretical properties (such as the NewWave profile).

The relatively low sampling frequency of 1.28 Hz may cause errors in the identification of the conditioning point in time, and hence in the ability to create average profiles with phases separated by exactly 180° (by creating a phase shift $\omega\Delta t$). This may cause some second-order contributions to remain within the 'linearised' profiles. However, the linearised profiles presented

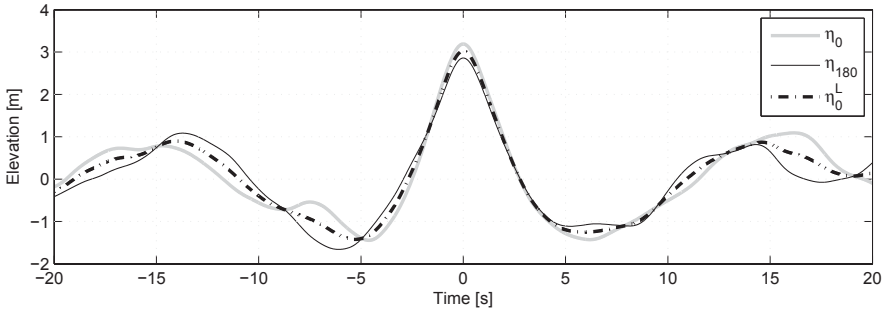

Figure 4: Average profiles calculated from the largest 20 crests and (inverted) troughs of Record 1a, and the linearised average large crest profile.

in this section exhibited excellent agreement with the NewWave profile despite the coarse data sampling.

Figure 4 compares the average profiles η_0, η_{180} and the linearised profile η_0^L. The average large trough profile is inverted to more clearly illustrate the differences in the amplitude and shape of the average large wave profiles. On visual inspection, the shapes of the three profiles are similar. Some small phase discrepancies are expected due to the relatively low sampling frequency. The separation of harmonics process slightly reduces the variability in the linearised profile by effectively doubling the number of waves contained within the average profile. Thus, the linearised profiles used in this section are expected to exhibit less variability than the nonlinear average large wave profiles considered in Section 4.

The larger amplitude of η_0 (compared to η_{180} and η_0^L) is consistent with the presence of second-order sum contributions to the average profiles, which lead to an increased crest height and a reduced trough height. Any difference contributions are assumed to have been removed by the high-pass filtering of the original records. To more closely investigate the nonlinearity of the waves within Record 1a, Figure 5 shows an ordered plot of the crest and trough amplitudes in the measured time series. For waves with amplitudes greater than approximately 1.5 m, the majority of the wave crests had slightly higher amplitudes than the troughs. This is typical of weakly nonlinear sea states where crests are slightly raised and troughs slightly reduced. By taking the Hilbert transform of the measured time series, introducing a 90° phase shift so that maxima and minima become zero-crossings, the departures from the 1:1 line for amplitudes greater than 1 m are substantially reduced (as discussed in Taylor and Williams, 2004; Santo et al., 2013). However, the reduced number of samples at the larger amplitudes still leads to larger variability at these amplitudes.

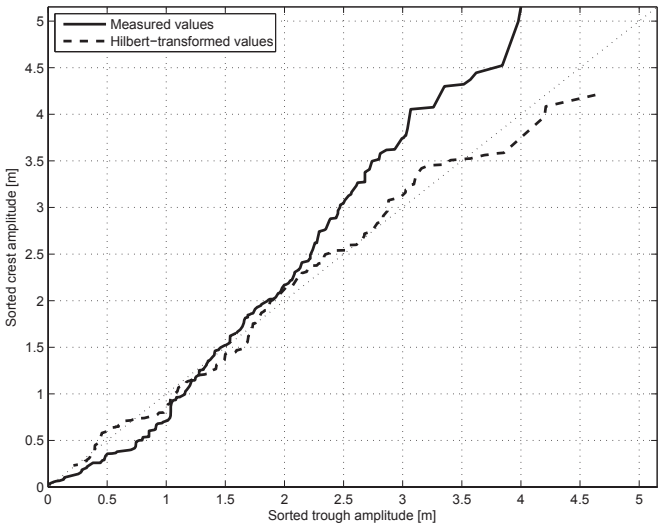

Figure 5: Sorted crest and trough amplitudes from Record 1*a* (and its Hilbert transform), showing departures from the 1:1 slope caused by wave nonlinearity.

3.2. The NewWave profile

The scaled autocorrelation function (i.e. the NewWave profile, y_0^1) is the asymptotic form of the full solution of Lindgren (1970) for the average shape of a large event within a random Gaussian process. This asymptotic form is valid for a wave amplitude α sufficiently large compared to the standard deviation of the process σ. Although the required wave amplitude (or crest size) is a weak function of the spectral bandwidth, the conservative value of 2σ will be used in this paper to determine the applicability of the autocorrelation function (Taylor and Williams, 2004). As stated previously, the average large wave profiles were created from the largest 20 waves in each record. The amplitude of the 20th-largest wave (3.49 m) was approximately 25% larger than $2\sigma \sim 2.80$ m, confirming the applicability of the autocorrelation function for the average profiles.

The NewWave profile is initially compared to the linearised average large wave profiles, to determine its ability to capture the features of large (albeit approximately linearised) waves in relatively shallow water. Neglecting the $k_i x$ term related to spatial dependence, this profile is given by:

$$y_0^1(t) = \alpha r_t = \frac{\alpha}{\sigma^2} \sum_{i=1}^{N} S_{\eta\eta}(\omega_i) \cos(\omega_i t) \Delta\omega, \tag{2}$$

where α is the maximum (linear) amplitude of the wave group, σ is the standard deviation of the sea state, $S_{\eta\eta}$ is the power spectral density and ω_i is the angular frequency. In this discretised

form, the surface variance is given by $\sigma^2 = \sum S_{\eta\eta}(\omega_i)\Delta\omega$.

When using NewWave as a design tool within large-scale hydraulic experiments or simulations, the total focused wave amplitude α may be set to correspond to a 1 in N event. This amplitude may be based on an assumed Rayleigh distribution of N individual wave amplitudes, requiring the assumption of a relatively narrow-banded spectrum (or a more generalised spectrum, as discussed by Tucker and Pitt, 2001). When comparing the profile to (linearised) measured data, α is set equal to the maximum amplitude of the linearised large crest profile η_{0L}. Thus, comparisons between y_0^1 and η_0^L demonstrate the ability of the linear NewWave profile to capture the average shape of the large waves measured by the wave buoys.

The range of kD values for the Perranporth and Porthleven buoy records provides a robust test of the NewWave profile's ability to replicate the average shape of large waves in relatively shallow water during storm events. Figure 6 compares the linear NewWave profile y_0^1 to the linearised average large crest profile η_0^L for the four records of interest. In this figure, each row corresponds to one of the two storms, while the columns correspond to different locations.

Following Santo et al. (2013), the fit between the NewWave profile and the linearised average large crest profile may be assessed by defining a tolerable level of mismatch. For this purpose, the 'Lindgren variance' (Lindgren, 1970) is used to calculate the standard deviation from the (expected) NewWave profile. The Lindgren variance is zero at the conditioning point, since it assumes that all waves used to create the average profile have an amplitude of α, and increases to the variance in the sea state within several wave periods of the conditioning point. Since the waves contributing to the average profiles did not have the same amplitude, a small amount of variability is also expected at the conditioning point.

The Lindgren variance is defined as:

$$Var_L(t) = \sigma^2 \left(1 - r_t^2 - \frac{\left(1/\sigma^2 \int \omega^2 S_{\eta\eta}(\omega) \sin(\omega t) d\omega\right)^2}{1/\sigma^2 \int \omega^2 S_{\eta\eta}(\omega) d\omega} \right), \tag{3}$$

where $\sigma = H_s/4$ is the standard deviation of the sea state, and $1/\sigma^2 \int \omega^2 S_{\eta\eta}(\omega) \sin(\omega t) d\omega$ is related to the autocorrelation function for the vertical velocity in the wave. The standard deviation illustrated in Figure 6 is $2\sigma_L$ (providing approximately 95% confidence intervals on the mean profiles), where σ_L is the Lindgren standard deviation $\sqrt{Var_L}$ divided by $\sqrt{N-1}$ (to assess deviations from the estimated mean of the profiles) and $N = 20$ is the number of large waves included.

Despite the (minor) differences in the shape of the average profiles and the possible effects of

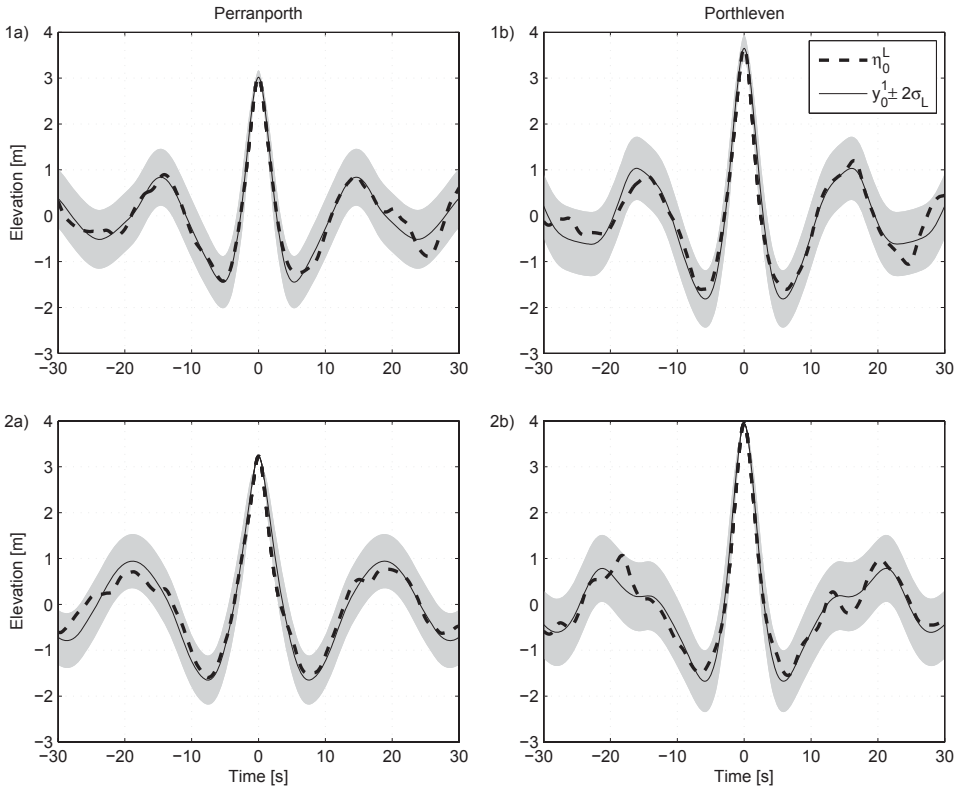

Figure 6: Ability of (linear) NewWave profile y_0^1 to represent the linearised average large crest profiles η_0^L for Records 1*a*-2*b*, using the Lindgren variance σ_L to calculate the standard deviation of the NewWave profile.

wave breaking, the NewWave profile closely matched the linearised average large crest profiles from the six records. As mentioned previously, the increased size of the Lindgren variance away from the conditioning point indicates the reduced confidence in predicting the average shape of the waves at longer times. Although the profiles exhibited some discrepancies with the linear NewWave profile away from the conditioning point, all of the average large crest profiles were contained within the $\pm 2\sigma_L$ confidence intervals. The discrepancies are expected to be larger for the waves with either the lowest kD values (due to the increased effect of the local bathymetry) or the largest amplitudes (due to the increased nonlinearity and the possibility of white-capping). However, the differences due to kD and amplitude were relatively minor, and all of the profiles exhibited excellent agreement with the linear NewWave profile.

Although the NewWave profile has been demonstrated to capture the properties of locally linearised large crests and troughs in relatively shallow water, the frequency spectrum $S(\omega)$ required to construct the NewWave profile may not be available at all locations of interest. For ocean engineering applications, the lack of field data often necessitates the use of empirical spectral models. We now compare the NewWave profiles calculated from two idealised spectral shapes (JONSWAP and TMA-transformed JONSWAP) to the NewWave profile calculated from Record 1*b*, demonstrating the effect of different spectral shapes on the resultant NewWave profile.

The JONSWAP spectrum is a commonly used spectrum derived from average fits to a large number of field observations from fetch-limited seas. Since this spectrum is valid for deep water, the TMA transformation is used to calculate the change in this spectrum as waves propagate into shallow water. The result of this transformation (see Holthuijsen, 2007) may be expressed as:

$$S(f)_D = \frac{S(f)_\infty}{2n} \tanh^2 kD, \tag{4}$$

where $S(f)_D$ is the depth-limited variance density spectrum, $S(f)_\infty$ is the deep-water variance density spectrum and n is the ratio of group velocity over phase velocity at depth D. In this case, $S(f)_\infty$ is taken to be a JONSWAP spectrum ($\gamma = 3.3$) with a peak frequency equal to 0.06 Hz (as measured by the E1 buoy shown in Figure 1), and the TMA transformation is used to calculate the spectral shape at the water depth of the study location. Figure 7 compares the idealised and measured spectral shapes, where the different spectra are normalised by their maximum values. Since the autocorrelation function is scaled by the desired linear amplitude α in Equation 2, this does not affect the resulting NewWave profiles.

Although the measured spectrum contains larger energy concentrations at frequencies equal to

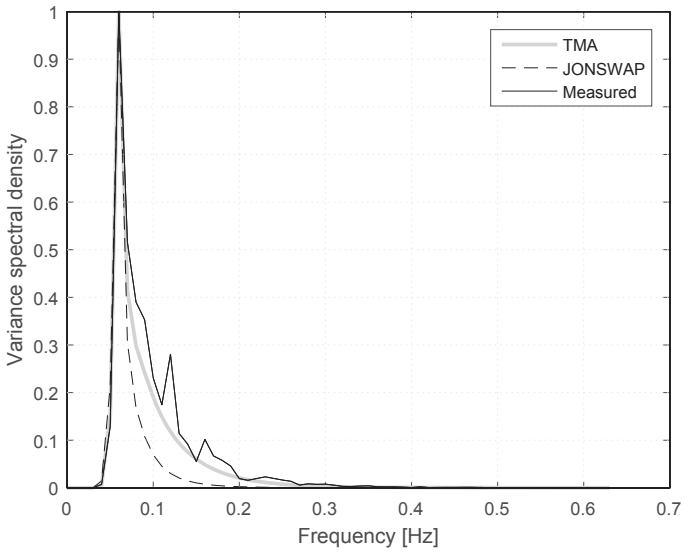

Figure 7: Similarity between the idealised TMA spectrum, the idealised JONSWAP spectrum and the measured spectrum from Record 1*b*. The spectra have all been normalised by their maximum variance spectral density, so that their shapes are more readily comparable.

approximately $2f_p$ and $3f_p$, the spectral shape is broadly similar to that of the TMA-transformed JONSWAP spectrum (including the high-frequency tail above approximately 0.2 Hz). However, the JONSWAP spectrum contains a much narrower peak than the other two spectra. This shows the importance of considering the water depth when calculating an idealised spectrum for a location where field data may not be available.

The JONSWAP and TMA-transformed spectra of Figure 7 was used to create NewWave profiles according to Equation 2, denoted $y_0^{JONSWAP}$ and y_0^{TMA} respectively. Figure 8 compares the NewWave profile from the two spectra to the NewWave profile created from the measured data of Record 1*b*. The Lindgren variance (Lindgren, 1970) again provides the standard deviations from the expected NewWave profile.

The NewWave profile calculated from the TMA spectrum shows excellent agreement with the NewWave profile calculated from the field data, and is entirely contained within the $\pm 2\sigma_L$ interval. This demonstrates that noise on a spectrum, and indeed slight differences in spectral shapes, do not affect the subsequent autocorrelation. These results provide confidence in the use of idealised spectra (of appropriate shapes) to predict the average shapes of large waves in relatively shallow water. The profile calculated from the JONSWAP spectrum lies outside of

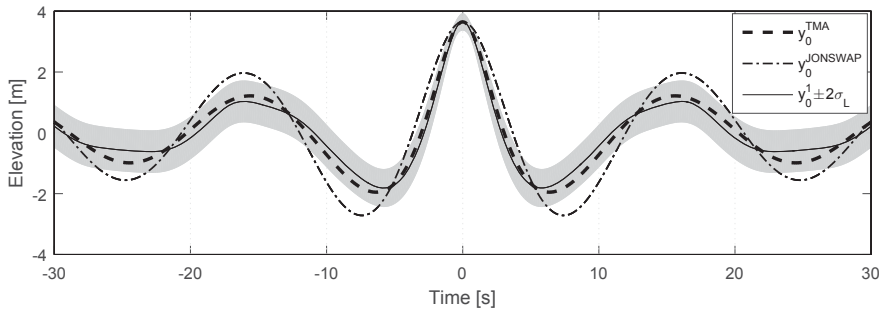

Figure 8: NewWave profiles resulting from the TMA and JONSWAP spectra, and comparison with the NewWave profile calculated from Record 1*b*.

this interval, and exhibits a slower amplitude decay away from the conditioning point due to the narrower spectral shape. These differences are unsurprising, given the differences between the spectral shapes. However, the results for measured and idealised spectra certainly support the use of the NewWave profile for large (pre-breaking) waves in the coastal zone.

4. Second-order additions to the NewWave representation of nonlinear wave profiles

4.1. Nonlinear corrections to the NewWave profile

Since the waves of most interest for engineering design are significantly nonlinear, several previous studies have investigated the possibility of adding nonlinear contributions to the NewWave profile. For example, Walker et al. (2004) used a 5th-order corrected NewWave to approximate the New Year Wave measured at the Draupner platform on 1 January 1995. Since steep shallow water waves will contain significant nonlinear contributions, a nonlinear-amended NewWave may be more appropriate in capturing the average properties of the largest (and most vertically asymmetric) waves measured at Perranporth and Porthleven. Only sum harmonic contributions are included in this correction, since the removal of low-frequency energy during the quality control processing of the buoy data is assumed to have removed the low-frequency second-order contributions to the nonlinear wave profiles.

Several different methods exist for the calculation of the second-order sum harmonic corrections to the linear NewWave profile. Walker et al. (2004) approximated the second-order corrected NewWave profile based on a Stokes expansion:

$$y_0^2 = y_0^1 + \frac{S_{22}}{D}((y_0^1)^2 - (y_0^H)^2), \tag{5}$$

where y_0^H is the Hilbert transform of the linear NewWave profile y_0^1, D is the water depth and S_{22} is the modified second-order Stokes coefficient. This is related to the more familiar Stokes coefficients by $S_{22}/D = kB_{22}$ (see the appendix of Walker et al., 2004, for the re-written Stokes theory up to fifth order). Although the linear NewWave profile is independent of bandwidth, the Walker approximation assumes that this linear profile is relatively narrow-banded. The shape of the correction term is independent of the dimensionless water depth k_pD.

An alternative more rigorous approach is to use the exact second-order superharmonic solution of Dalzell (1999) and Forristall (2000), based on the original solution of Sharma and Dean (1981) for second-order wave-wave interactions (but with minor typographical errors removed). However, the advantage of the simpler approximation is that it may be readily extended to include higher orders or the effects of the Lagrangian buoy motion. To determine the validity of the approximate method at second order, the Walker correction is compared to the superharmonic solution of Dalzell (1999). Figure 9 shows these comparisons for idealised JONSWAP spectra with k_pD values of 0.5, 1.0 and 1.5, where the profiles are all normalised by their maximum amplitude. Although this spectrum is narrower than the measured spectra, the largest waves within a sea state (i.e. those with the greatest contribution to the second-order profile) may be assumed to be narrow-banded (Tucker and Pitt, 2001). The effects of the buoy motion ('Lagrangian Walker approx.') are discussed in Section 4.2.

At the k_pD values of 1.0 and 1.5, the Walker approximation is almost indistinguishable from the full second-order solution of Dalzell (1999). The differences between the two profiles become more pronounced at $k_pD = 0.5$, although the discrepancies in the vicinity of the conditioning point (of greatest interest due to the vanishing Lindgren variance) are still minor. It should be noted that the narrow-banded Walker approximation would not be valid for a spectrum with two dominant frequencies. However, this approximation works well for even the relatively broad-banded spectra investigated in this paper.

4.2. Effects of Lagrangian buoy motion in relatively shallow water

Wave buoys are often employed for field measurements of water waves in the absence of a supporting structure (precluding most surface-piercing measurement devices). An advantage of wave buoys over wave gauges (more traditionally used in large-scale hydraulic experiments) and bottom-mounted pressure sensors is that they can provide information on wave direction and amplitude. However, this comes at the cost of reduced nonlinear contributions. Before applying our Eulerian second-order analysis to wave buoy data, we consider the effects of the buoy motion

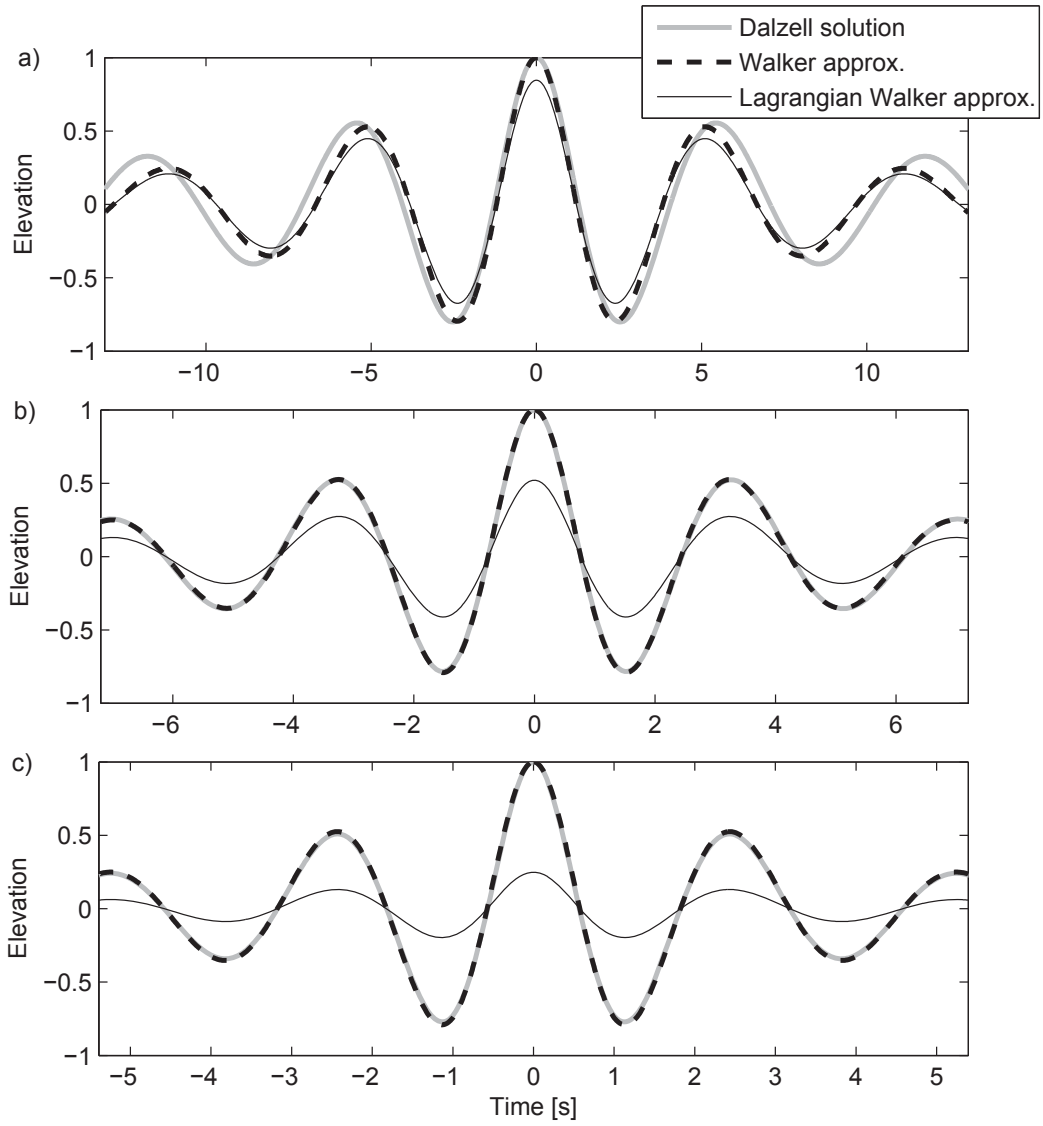

Figure 9: Comparison between the full second-order solution of Dalzell (1999) and the second-order sum harmonic approximation of Walker et al. (2004) for a) $k_pD = 0.5$, b) $k_pD = 1.0$ and c) $k_pD = 1.5$, all for the same linear NewWave group.

on the nonlinear contributions to the measured surface elevations.

As mentioned in Section 2, even a 'perfect' surface-following buoy will record Lagrangian rather than Eulerian motion since it will spend longer in a crest than a trough (Tucker and Pitt, 2001). Thus, the crests within the measured time series will be broader than those measured by an Eulerian sensor, while troughs will be relatively sharpened. The increased time spent in wave crests also results in a setup of the apparent mean free surface level measured by the buoy. For regular waves measured in deep water, the motion of a Lagrangian sensor prevents it from measuring the second-order Eulerian fluid motions (and hence the second-order contribution to the surface waves, as discussed in Longuet-Higgins, 1986). However, this effect changes in intermediate and shallow water depths. Considering a regular wave group in finite water with free surface elevation given by:

$$y = a\cos(kx - \omega t) + \frac{a^2 S_{22}}{D}\cos(2\,(kx - \omega t)), \tag{6}$$

the Eulerian time history of wave elevation (at $x = 0$) is:

$$y_E = a\cos(\omega t) + \frac{a^2 k\cos(2\omega t)\,(2 + \cosh(2kD))\coth(kD)\,\mathrm{csch}^2\,(kD)}{4}. \tag{7}$$

The Lagrangian time history can be found by substituting the linear approximation of the horizontal displacement $y_H = -a\sin\omega t$ into Equation 6 and expanding to second order in the amplitude a, giving:

$$\begin{aligned} y_L &= a\cos(\omega t) \\ &- \frac{a^2\coth(kD)\left(kD\cos(2\omega t) + 2kD\sin(\omega t)^2 + 2\,\mathrm{sech}(2kD)\left(kD\cos(2\omega t) - kD\sin^2(\omega t)\right)\right)}{2D\,(-1 + \mathrm{sech}\,2kD)}. \end{aligned} \tag{8}$$

where kD is the nondimensional water depth for regular waves of wave number k and angular frequency ω. As expected, the linear terms $a\cos(\omega t)$ in the Eulerian and Lagrangian time series are equal. After removing these linear terms, the apparent setup of the mean free surface level in the Lagrangian time series (see Longuet-Higgins, 1986) should also be removed. This apparent setup is caused by the buoy spending more time in a crest than a trough, where (as well as broadening crests and steepening troughs in the measured time series) the average position of the buoy is slightly elevated, and is given by:

$$\overline{y_L} = \frac{a^2 kD\coth kD}{2D}. \tag{9}$$

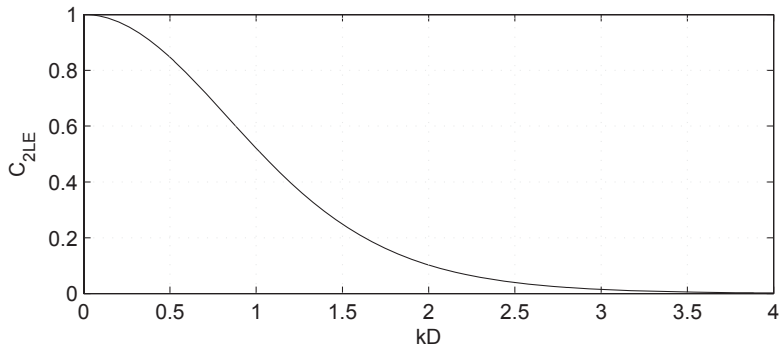

Figure 10: Dependence of the ratio between the second-order term measured by a Lagrangian and Eulerian sensor (C_{2LE}) on the nondimensional water depth in regular waves.

After removing this setup, the ratio between the second-order Lagrangian and Eulerian double-frequency terms is given by C_{2LE}, where:

$$C_{2LE} = \frac{3}{2 + \cosh 2kD}. \tag{10}$$

The physical explanation for the ratio between the Eulerian and Lagrangian measurements is that as the water depth decreases, the horizontal distance travelled by a wave buoy increases relative to its vertical displacement. Thus, the effects of the Lagrangian buoy motion become stronger in shallower water. However, the size of the second-order (sum) Stokes corrections to a linear wave profile also increase as the depth approaches the shallow water limit. The effect of the increased size of the Stokes corrections is larger than the effect of the buoy motion in shallow water, with the result that a Lagrangian sensor in very shallow water will measure the complete second-order Stokes sum contribution to the free surface elevation. Figure 10 illustrates the dependence of this ratio on kD.

Clearly, a buoy in intermediate or moderately shallow water will measure a non-negligible fraction of the Eulerian second-order sum contribution to a regular wave group, the proportion being reduced from unity according to Equation 10. Assuming that the linear NewWave profile is relatively narrow-banded in frequency, the approximation for the second-order corrections to the NewWave profile in Walker et al. (2004) may be adjusted to account for the effects of the Lagrangian buoy motion as follows:

$$y_0^2 = y_0^1 + \frac{S_{22}}{D}((y_0^1)^2 - (y_0^H)^2)\left(\frac{3}{2 + \cosh 2kD}\right), \tag{11}$$

where in this case a representative kD value may be obtained based on the magnitude of S_{22} (discussed below). Applying Equation 11 will result in a reduction of the Eulerian second-order correction to the NewWave profile, making it appropriate for comparison with the measurements of a Lagrangian wave buoy. The effect on the second-order contributions to the measured waves are shown in Figure 9, where the amplitude reductions due to the buoy motion associated with $k_pD = 0.15, 1.0$ and 1.5 are 0.85, 0.52 and 0.25 respectively. The records of interest in this study are closest to the case $k_pD = 0.5$, and hence the second-order sum contributions to the wave elevations recorded by the wave buoy should be clearly visible.

In an analysis of the New Year Wave recorded at the Draupner Platform, Walker et al. (2004) selected the S_{22} coefficient by linearising the measured time series using a variation of Equation 5 and setting the skewness of the linearised time series to zero. The S_{22} value obtained in this way corresponded to a kD value of approximately 1.6, and was relatively insensitive to small changes in kD. However, the lower kD values in the current study make the S_{22} value much larger and more sensitive to small changes in kD. Thus, the S_{22} coefficient was instead obtained by setting the maximum amplitude of the Walker approximation to the second-order sum correction equal to the exact second-order superharmonic solution of Dalzell (1999) at $t = 0$ s (the central crest location). The effective kD value corresponding to this net S_{22} value was then calculated and used to correct the Walker approximation for the Lagrangian wave buoy motion.

The modified Walker approximation will be used to amend the NewWave profile for second-order effects, creating the second-order NewWave profile to be fitted to nonlinear average large wave profiles in the next section. Although directional spreading may also affect the second-order sum contributions (see Forristall, 2000), this effect is not considered in the present analysis of heave motions (it is likely that the directional spreading in deep water would have been reduced due to refraction as the waves entered progressively shallower water). The effects of the mooring on the buoy motion are also not considered in the current study.

4.3. Amended NewWave representation of nonlinear wave profiles

We now fit a second-order amended NewWave profile to the average large crest and trough profiles. The sum harmonic contributions are approximated using the method of Walker et al. (2004), modified for the Lagrangian buoy motion as discussed in Section 4.2. The S_{22} coefficient is evaluated using the appropriate wave spectrum and the full solution of Dalzell (1999). Using this method, both the amplitude and phase of the linear NewWave profile are adjusted to achieve the optimal fit to the average large wave profile. A phase-shifted linear NewWave may be constructed

as:

$$y_\phi^1(t) = \frac{\alpha}{\sigma^2} \sum_{i=1}^{N} S_{\eta\eta}(\omega_i) \cos(\omega_i t - \phi) \Delta\omega, \tag{12}$$

where ϕ is the total phase shift applied to the NewWave profile. Note that α is still the maximum amplitude of the zero-phase NewWave profile, and therefore may not be the maximum amplitude of the phase-shifted profile (though it is the maximum value of the envelope of this wave group). Due to the uncertainty regarding the 'correct' linear amplitude and phase of the NewWave profile, a range of linear NewWave amplitudes and phases are tested and optimised using a weighted least-squares fit to the profile of interest. The fit to the profile is weighted by the envelope of the linear NewWave profile, since it is only in the vicinity of the conditioning point ($t = 0$ s) that the Lindgren variance is less than the variance of the sea state. Far enough from the conditioning point, knowledge about the large event (crest/trough) does not provide any information about the expected shape of the free surface, and a zero weighting is appropriate.

Figure 11 shows the effectiveness of the NewWave fit for the four records from Perranporth and Porthleven, showing both the linear and nonlinear NewWave profiles. The confidence intervals in the nonlinear NewWave profile are again estimated using $2\sigma_L$. The agreement with the nonlinear NewWave profile is still good. These (nonlinear) average profiles were not linearised using the separation of harmonics analysis of Section 3, so the greater variability in the profiles of Figure 11 (containing 20, not 40, waves) is expected.

Figure 12 shows the NewWave fits to the average large trough profiles. The fits are poorer than for the average large crest profiles, and the second-order corrected NewWave profiles show pronounced reductions in the amplitude of the central trough. The occurrence of localised 'wiggles' at the troughs of a steep shallow water wave train is a well known effect of not including enough harmonics in a Stokes expansion. The convergence of the Stokes expansion is relatively poor in very shallow water, and theoretical results for regular waves indicate that the 'secondary crests' are a consequence of not including the 3rd harmonic in the analysis. However, the correction to the 2nd harmonic based on the Lagrangian buoy motion does not work at 3rd order (and a 3rd-order analysis is generally much more complicated for irregular sea states). Thus, in this work we only include the fundamental and second harmonic.

The calculation of the S_{22} coefficients during the optimisation process also enables an effective kD value to be calculated for each of the 'optimal' nonlinear NewWave profiles. These effective values, listed in Table 3, were all located between the kD values calculated using the peak wavenumber and the average wavenumber (listed in Table 2). The phases of the linear NewWave

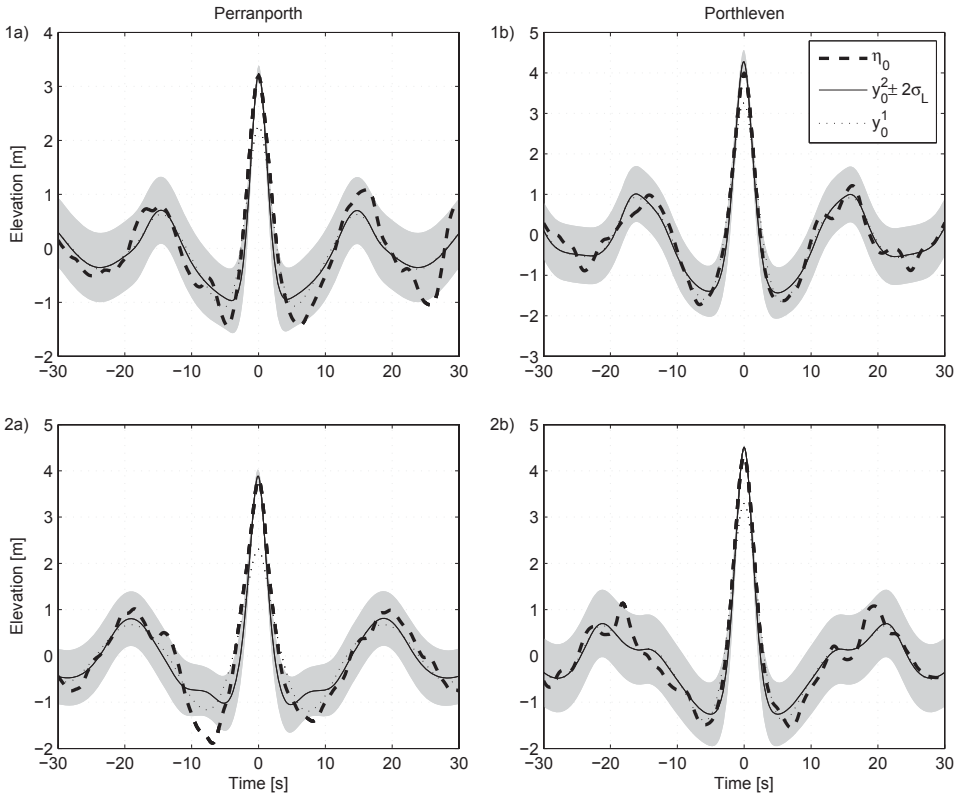

Figure 11: Ability of nonlinear-corrected NewWave profile y_0^2 to represent the average large crest profiles η_0 for Records 1*a*-2*b*, using the Lindgren standard deviation $2\sigma_L$ to assess the quality of fit. The linear NewWave profile y_0^1 is shown for reference.

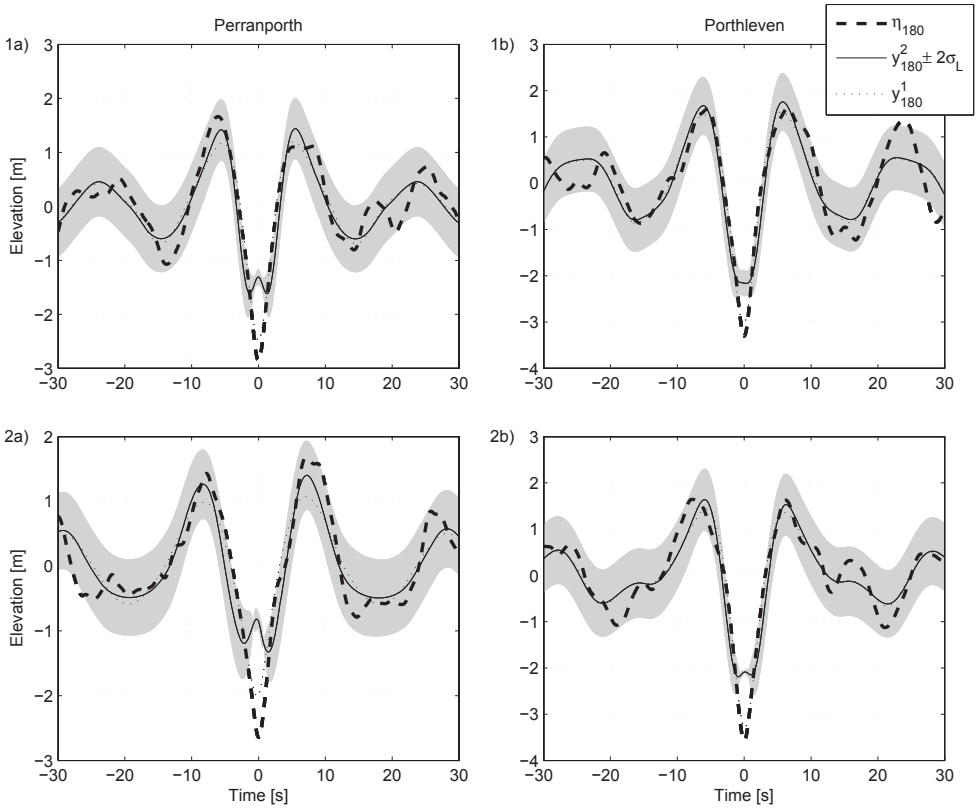

Figure 12: Ability of nonlinear-corrected NewWave profile y^2_{180} to represent the average large trough profiles η_{180} for Records 1*a*-2*b*, using the Lindgren standard deviation $2\sigma_L$ to assess the quality of fit. The linear NewWave profile y^1_{180} is shown for reference.

Table 3: Effective kD values calculated from the S_{22} coefficients (used to correct the NewWave profiles for second-order sum contributions), and linear NewWave phases required for optimised second-order fit to average large wave profiles.

Record no.	kD for y_0	kD for y_{180}	ϕ for y_0	ϕ for y_{180}
1a	0.62	0.62	2°	179°
2a	0.50	0.50	-3°	170°
1b	0.71	0.72	-3°	176°
2b	0.67	0.67	0°	184°

group, ϕ, are also shown for the two cases. Phase departures from $\pm 180°$ may, of course, be partly due to the sparsely sampled surface elevation data, since the maximum elevation may have occurred within $\pm\Delta t$ of the conditioning point $t = 0$ s. This corresponds to a phase shift of up to $\omega_p \Delta t = 15°$ for the wave buoy data, which is larger than the observed shifts from 0° and 180° listed in Table 3.

These results demonstrate that a nonlinear-amended NewWave profile with appropriate linear phase and amplitude properties is able to capture the average properties of (weakly nonlinear) large waves in relatively shallow water.

5. Conclusions

The NewWave profile has been demonstrated to accurately replicate the (linearised) average shapes of large waves measured at Perranporth and Porthleven during two of the large storms recorded during January 2014. This agreement is observed even down to kD values of approximately 0.4, much shallower water than has been investigated in previous studies comparing NewWave to field data. The success of the NewWave profile provides confidence in the application of localised wave group structures such as NewWave to drive inshore flows responsible for runup on a beach, overtopping of sea defences or loading of coastal structures.

The simple sum harmonic corrections of Walker et al. (2004) were shown to be effective in reproducing the second-order sum harmonic perturbation expansion solutions of Dalzell (1999). The Lagrangian motion of a wave buoy is shown to reduce the second-order sum harmonic contribution in its measured signal, and a simple method is presented to account for these in the Walker solution. This correction depends on the nondimensional water depth kD, and varies between unity (no reduction in second-order sum harmonics) for shallow water and zero (all second-order sum harmonics eliminated) in deep water. Using these nonlinear corrections, a

second-order corrected NewWave profile (optimised for linear phase and amplitude) was able to provide a reasonable approximation to the (nonlinear) average large crest and trough profiles.

The results presented in this paper provide confidence in the application of NewWave to hydraulic problems in relatively shallow-water conditions. Indeed, focused wave groups in general (and the NewWave profile in particular) have been successfully used in some large-scale coastal experiments (Martinelli et al., 2011; Lamberti et al., 2010). Future investigations will determine whether the extreme responses of coastal structures within long-duration irregular wave tests can be replicated by an extreme incident wave group.

Acknowledgements

This work was conducted within the ENFORCE (Extreme Responses using NewWave: Forces, Overtopping and Runup in Coastal Engineering) project, under EPSRC Grant EP/K024108/1. The authors gratefully acknowledge the assistance of the staff of the Plymouth Coastal Observatory (PCO) in obtaining the wave buoy data.

Nomenclature

Note: A p subscript refers to the peak value, while a z subscript for a variable refers to the average value.

t	Time (s)
D	Depth (m)
ω	Angular frequency (rad/s)
f	Frequency (Hz)
k	Wavenumber (m^{-1})
λ	Wavelength (m)
H_s	Significant wave height (m), where $H_s = 4\sigma$ by definition
H_{max}	Maximum pre-breaking wave height (m)
T	Period (s)
$S_{\eta\eta}$	Power spectral density
σ^2	Variance of sea state
α	Amplitude of linear NewWave group
ϕ	Phase of linear NewWave group
η	Free surface amplitude
η_ϕ	Average large wave profile with phase ϕ
η_ϕ^L	Linearised average large wave profile with phase ϕ
y_ϕ^1	Linear NewWave profile with phase ϕ at focus
y_ϕ^H	Hilbert-transformed linear NewWave profile with phase ϕ at focus
y_ϕ^2	Second-order amended NewWave profile with phase ϕ at focus
n	Ratio of group velocity to phase velocity
S_{22}	Modified Stokes coefficient for second-order sum harmonic in regular waves
a	Amplitude of regular wave group
y_H	Horizontal displacement within a regular wave group
y_E	Eulerian free surface elevation measurement
y_L	Lagrangian free surface elevation measurement
C_{2LE}	Ratio between the second-order Lagrangian and Eulerian double-frequency terms
σ_L	Lindgren standard deviation about average profile

References

References

Adcock, T.A., Taylor, P.H., 2014. The physics of anomalous ('rogue') ocean waves. Reports on Progress in Physics 77, 105901.

Ashton, I., 2012. Spatial variability of wave fields over the scale of a wave energy test site. D.Phil.. University of Exeter (United Kingdom).

Ashton, I., Johanning, L., 2015. On errors in low frequency wave measurements from wave buoys. Ocean Engineering 95, 11 – 22. doi:http://dx.doi.org/10.1016/j.oceaneng.2014.11.033.

Boccotti, P., 1983. Some new results on statistical properties of wind waves. Applied Ocean Research 5, 134 – 140. doi:http://dx.doi.org/10.1016/0141-1187(83)90067-6.

Constantin, A., 2014. Estimating wave heights from pressure data at the bed. Journal of Fluid Mechanics Rapids 743.

Dalzell, J., 1999. A note on finite depth second-order wavewave interactions. Applied Ocean Research 21, 105 – 111. doi:http://dx.doi.org/10.1016/S0141-1187(99)00008-5.

Forristall, G.Z., 2000. Wave crest distributions: Observations and second-order theory. Journal of Physical Oceanography 30, 1931–1943.

Geeraerts, J., Troch, P., Rouck, J.D., Verhaeghe, H., Bouma, J., 2007. Wave overtopping at coastal structures: prediction tools and related hazard analysis. Journal of Cleaner Production 15, 1514 – 1521. doi:http://dx.doi.org/10.1016/j.jclepro.2006.07.050. water Management in Coastal Zones and Deltas.

Hofland, B., Wenneker, I., Van Steeg, P., 2014. Short test durations for wave overtopping experiments, in: Proceedings of the 5th International Conference on the Application of Physical Modelling to Port and Coastal Protection, pp. 349–358.

Holthuijsen, L.H., 2007. Waves in Oceanic and Coastal Waters. Cambridge University Press.

James, I., 1986. A note on the theoretical comparison of wave staffs and waverider buoys in steep gravity waves. Ocean Engineering 13, 209–214.

Janssen, P.A., 2003. Nonlinear four-wave interactions and freak waves. Journal of Physical Oceanography 33, 863–884.

Jonathan, P., Taylor, P.H., 1997. On irregular, nonlinear waves in a spread sea. Journal of Offshore Mechanics and Arctic Engineering 119, 37–41. 10.1115/1.2829043.

Lamberti, A., Martinelli, L., Guerrero, M., Gaeta, G., Allsop, W., Alderson, J., Tirindelli, M., Shepsis, V., Hunt-Raby, A., Sellar, B., et al., 2010. Large scale measurements of extreme wave loadings on exposed jetties, in: Proc. HYDRALAB III Joint User Meeting, Hannover, pp. 45–48.

Lindgren, G., 1970. Some properties of a normal process near a local maximum. The Annals of Mathematical Statistics 41, pp. 1870–1883.

Longuet-Higgins, M.S., 1986. Eulerian and Lagrangian aspects of surface waves. Journal of Fluid Mechanics 173, 683–707.

Martinelli, L., Lamberti, A., Gaeta, M.G., Tirindelli, M., Alderson, J., Schimmels, S., 2011. Wave loads on exposed jetties: description of large scale experiments and preliminary results. Coastal Engineering Proceedings 1, 18.

Pullen, T., Allsop, N.W.H., Bruce, T., Kortenhaus, A., Schüttrumpf, H., van der Meer, J.W., 2007. EurOtop Wave overtopping of sea defenses and related structures - Assessment manual. URL: http://www.overtopping-manual.com/europtop.pdf.

Santo, H., Taylor, P.H., Eatock Taylor, R., Choo, Y.S., 2013. Average properties of the largest waves in Hurricane Camille. Journal of Offshore Mechanics and Arctic Engineering 135, 1–7.

Scott, T., Masselink, G., Russell, P., 2011. Morphodynamic characteristics and classification of beaches in England and Wales. Marine Geology 286, 1 – 20. doi:http://dx.doi.org/10.1016/j.margeo.2011.04.004.

Sharma, J.N., Dean, R.G., 1981. Second-order directional seas and associated wave forces. Society of Petroleum Engineers Journal 21, 129–140. doi:http://dx.doi.org/10.2118/8584-PA.

Taylor, P.H., Williams, B.A., 2004. Wave statistics for intermediate depth water - NewWaves and symmetry. Journal of Offshore Mechanics and Arctic Engineering 126, 54–59. 10.1115/1.1641796.

Tromans, P.S., Anaturk, A.R., Hagemeijer, P., 1991. A new model for the kinematics of large ocean waves - application as a design wave, in: Proceedings of the First International Offshore

and Polar Engineering Conference, The International Society of Offshore and Polar Engineers. pp. 64–71.

Tucker, M.J., Pitt, E.G., 2001. Waves in Ocean Engineering. Elsevier.

Walker, D., Taylor, P., Taylor, R.E., 2004. The shape of large surface waves on the open sea and the Draupner New Year wave. Applied Ocean Research 26, 73 – 83. doi:http://dx.doi.org/10.1016/j.apor.2005.02.001.